Taylor & Francis
Taylor & Francis Group

RESEARCH ARTICLE

🔓 OPEN ACCESS   ⬤ Check for updates

Protective effect of Qingre Huoxue decoction against myocardial infarction via PI3K/Akt autophagy pathway based on UPLC-MS, network pharmacology, and *in vivo* evidence

Zheng Jin[a], Wenbo Zhang[b], Yuan Luo[c], Xiushen Li[d], Lijin Qing[e], Qiang Zuo[f], Junfeng Fang[g] ⓘ and Wei Wu[e] ⓘ

[a]ZhuJiang Hospital, Southern Medical University, Guangzhou, China; [b]Research Center of Integrative Medicine, School of Basic Medical Sciences, Guangzhou University of Chinese Medicine, Guangzhou, China; [c]The First Clinical Medical School, Guangzhou University of Chinese Medicine, Guangzhou, China; [d]Department of Obstetrics and Gynecology, Shenzhen University General Hospital, Shenzhen, China; [e]Department of Cardiovascular, First Affiliated Hospital of Guangzhou University of Chinese Medicine, Guangzhou, China; [f]First Affiliated Hospital, Anhui University of Chinese Medicine, Hefei, China; [g]Department of Emergency, First Affiliated Hospital of Guangzhou University of Chinese Medicine, Guangzhou, China

ABSTRACT

Context: Qingre Huoxue (QRHX) decoction, a traditional Chinese medicine, has been widely used to prevent and treat myocardial infarction (MI).

Objective: This study elucidates the possible mechanisms of QRHX in preventing or treating MI in a rat model.

Materials and methods: The chemical constituents of QRHX were identified by UPLC-MS. Sprague-Dawley rats were randomly divided into the Sham (normal saline), Model (normal saline), QRHX-L, QRHX-M and QRHX-H group ($n = 10$ per group). QRHX decoction was administered by gavage to the rats for 14 days (5, 10 and 20 g/kg/day). The left anterior descending ligation method was performed to develop MI in Model and QRHX groups, and the same surgical procedures excluding ligation sutures were performed for the sham group. Finally, we evaluated cardiac function, myocardial fibrosis degree, serum inflammatory factors, autophagy levels and verified the signalling pathways *in vivo*.

Results: A total of 68 active components of QRHX corresponding to 223 active targets were obtained and 2558 MI-related disease targets were collected. After integration, 123 QRHX anti-MI targets were obtained, and 70 signalling pathways, such as PI3K/Akt, were identified by enrichment analysis. *In vivo* experiments suggest that QRHX could reduce the degree of myocardial fibrosis, downregulate serum inflammatory factors, and promote autophagy in MI rats.

Discussion and Conclusions: QRHX plays a protective role in the myocardium by mediating PI3K/Akt signalling pathway to activate autophagy and inhibiting inflammatory factor expression. These findings provide a scientific basis for further research and validation of QRHX as a potential therapeutic for MI.

Introduction

Myocardial infarction (MI) is caused by a sudden decrease in coronary blood flow accompanied by continuous cardiac hypoxia, which results in myocardial necrosis. The Fourth Universal Definition of MI Consensus Document, released at the 2018 European Society of Cardiology annual meeting, describes the criteria for myocardial injury and MI including abnormal cardiac biomarkers confirming acute myocardial damage and clinical evidence of acute myocardial ischaemia (Thygesen et al. 2019). MI is a type of coronary heart disease associated with high morbidity, mortality and disability. Scientific and technological development has led to consistent improvements in MI treatment. Studies have shown that reperfusion therapy, percutaneous coronary intervention, antithrombotic therapy and secondary prevention could improve prognosis and reduce mortality of patients with MI (Roffi et al. 2016; Ibanez et al. 2018).

Despite advances in medical technology, stent restenosis after percutaneous coronary intervention and side effects caused by long-term use of antiplatelet therapy and statins remain concerning (Xiu et al. 2018). With the increasing influence of traditional Chinese medicine (TCM) in disease prevention and treatment, its use in cardiovascular diseases has also been increasing (Hao et al. 2017; Li and Zhao 2017). Studies have confirmed that a variety of TCM compounds have cardioprotective effects (Li et al. 2018; Jia et al. 2019; Fan et al. 2020). Qingre Huoxue (QRHX) decoction is a TCM formulation consisting of *Scutellaria baicalensis* Georgi (Lamiaceae), *Paeonia veitchii* Lynch (Paeoniaceae), *Ligusticum chuanxiong* Hort. (Apiaceae), *Ilicis pubescentis* Hook. & Arn. (Aquifoliaceae), *Carthamus tinctorius*

CONTACT Junfeng Fang ✉ gzyyfyfjf@163.com 🏢 Department of Emergency, First Affiliated Hospital of Guangzhou University of Chinese Medicine, No.16, Ji Chang Road, Baiyun, Guangzhou 510405, China; Wei Wu ✉ wwhrlz@163.com 🏢 Department of Cardiovascular, First Affiliated Hospital of Guangzhou University of Chinese Medicine, No.16, Ji Chang Road, Baiyun, Guangzhou 510405, China

🔓 Supplemental data for this article can be accessed here.

L. (Asteraceae), *Dalbergia odorifera* T. Chen (Fabaceae) and *Salvia miltiorrhiza* Bge (Lamiaceae). It has the effect of clearing heat (detoxification), promoting blood circulation and reducing blood stasis. However, the specific mechanism and target of anti-MI effects of QRHX remain unclear.

Different classes of cytokines produced inside the human body play a crucial role in MI inducement and progression, such as tumour necrosis factor α (TNF-α), interleukin-1β (IL-1β), monocyte chemoattractant protein-1 (MCP-1) and interleukin-17A (IL-17A). The pro-inflammatory cytokines, TNF-α and IL-1β, which are released as a stress response against myocardial injury (Mourouzis et al. 2020), have a significant pleiotropic effect on myocytes contributing to phenotype reprogramming or remodelling (Tousoulis et al. 2006). The upregulation of MCP-1 and IL-17A following MI, induces cytokine secretion of inflammatory cells, is associated with the inflammatory responses and the loss of function in post-MI hearts (Ren et al. 2003, Zhang, Liu, et al. 2019). Autophagy can act both as an inflammatory suppressor and a detrimental effect on the heart by excessive activation, indicating its controversial role (Bai et al. 2018; Wang et al. 2018). Many autophagy-related proteins are recognized to be involved in the process of MI, such as microtubule-associated protein light chain 3B (LC3B), Beclin-1, protein 62 (P62), autophagy-related protein 3 (ATG3), autophagy-related protein 5 (ATG5) and autophagy-related protein 7 (ATG7). LC3B is a marker being widely used to monitor autophagy activity, which can be determined by the ratio of LC3II/I (Escobar et al. 2013), while P62 is the associated negative regulating protein (Jiang et al. 2015). Beclin-1 serves as a marker of autophagosome and autolysosome fusion in MI (Emanuele et al. 2014). ATG3, ATG5 and ATG7 are also necessary autophagy proteins in cardiomyocytes, and their loss leads to cardiac dysfunction (Ma et al. 2015). It is known that B-cell lymphoma-2 (Bcl-2) significantly inhibits apoptosis, while B-cell lymphoma 2-Associated X (Bax) is an apoptotic gene that inhibits Bcl-2. The ratio of Bcl-2/Bax serves as a key factor in determining the degree of apoptosis, which is important in post-MI health management (Cai and Shen 2018).

Early inflammatory activation in the cardiac repair phase after MI is necessary for the transition to later reparative and proliferative programs. Inflammation that is disproportionately prolonged, of excessive magnitude, or insufficiently suppressed

promotes adverse remodelling. Moreover, inflammation is a key regulator for autophagy, and when excessive inflammation occurs, autophagy is inhibited and can thus act as an inflammatory inhibitor to reduce heart injury (Mohajeri and Sahebkar 2018; Ryter et al. 2019). Fibroblasts may respond to stimulation with danger-associated molecular patterns, acquiring a pro-inflammatory fibroblast phenotype, secreting more inflammatory cytokines and chemokines (Shinde and Frangogiannis 2014). Multiple pathophysiological factors promote the occurrence of myocardial fibrosis after MI, which may lead to heart failure.

It is challenging to explore the relationship between various active components of TCM and genes and signalling pathways. This research adopts the ultra-performance liquid chromatography-mass spectrometry (UPLC-MS) analysis and network pharmacology method to predict targets, which were then verified by *in vivo* experiments to explore the potential myocardial protection mechanism of QRHX more reasonably and provide a new direction for MI intervention and therapies. The workflow of this study is shown in Figure 1.

Materials and methods

Chemicals and reagents

Scutellaria baicalensis, No. H5369212, *Paeonia veitchii*, No. C2669212, were obtained from Guangdong medicinal herbs Company Herbal Medicine Factory (Foshan, China); *Ligusticum chuanxiong*, No. H5369212, was obtained from Guangdong Tiancheng Traditional Chinese Medicine Co., Ltd. (Jieyang, China). *Ilicis pubescentis*, No. 2006098, *Carthamus tinctorius*, No. 2008221, were obtained from Guangzhou Zihetang Pharmacy Co., Ltd (Guangzhou, China); *Dalbergia odorifera*, No. 200601, *Salvia miltiorrhiza*, No. 200801, were obtained from Zisun Chinese Pharmaceutical Co., Ltd (Guangzhou, China). The seven herbs were weighed and mixed in a proportion of 3:3:2:6:2:2:6 (Zuo et al. 2021). The active ingredients of the mixture were then extracted using water (1:6) twice under refluxing, 1 h per time. Afterward, the extracted solutions were combined, filtered and then concentrated using a rotary evaporator.

Cardiac Troponin I (cTnI) ELISA Kit (ab246529), MCP1 ELISA Kit (ab100777), IL-17A ELISA Kit (ab214028), TNF-α ELISA Kit (ab236712) and IL-1β ELISA Kit (ab255730) were
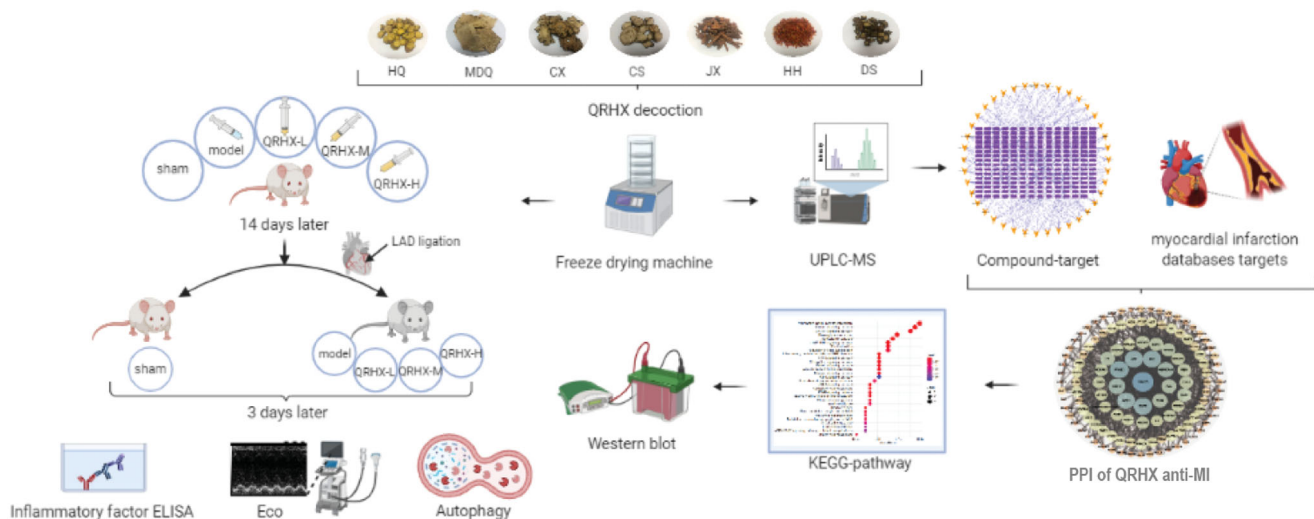

Figure 1. Study workflow.

obtained from Abcam (USA) and the BCA kit was purchased from Beyotime (China). HE staining Kit (G1120) was purchased from Solarbio (China). Masson's Trichrome Stain Kit (DC0032) and Picro Sirius Red Stain Kit (DC0041) were purchased from Leagene Biotechnology (China). A miRNeasy Micro Kit and M-MLV Reverse Transcriptase kits were purchased from Takara (Japan). The following antibodies p-PI3K (Abcam, ab182651), PI3K (CST, 4292), p-Akt (CST, 9271), Akt (ab179463), LC3B (ab192890), Beclin-1 (ab207612), P62 (ab155686), HRP (ab6734) and GAPDH (ab9485) were obtained from Abcam (USA).

Sample preparation and quality control

QRHX decoction was prepared by the Department of Pharmacy, the first affiliated Hospital of Guangzhou University of Traditional Chinese Medicine. Freeze-dried QRHX powder was obtained according to the method detailed above.

UPLC-MS analysis

Liquid chromatography was performed on an Agilent 1290 UPLC system (Agilent Technologies, USA) equipped with a binary pump, an auto-plate sampler, a thermostatically controlled column compartment and a diode array detection system. Detection was performed by an Agilent 6550 Q-TOF mass spectrometer (Agilent Technologies, USA). Chromatographic separation was conducted on an Agilent extend C18 (2.1×50 mm, 1.7 um). The mobile phase was composed of 0.1% formic acid solution (A) and acetonitrile solution (B), with a gradient elution procedure as follows: 0–1 min, 90% A, 10% B; 1–3 min, 10% A, 90% B; 1–3 min, 10% A, 90% B; 12–13 min, 90% A, 10% B. The flow rate was 0.3 mL/min, and the injection volume was 10 mL.

The MS spectra were acquired in both positive and negative ion modes to provide complementary information for structural identification. The acquisition parameters for Q-TOF mass spectra were as follows: drying gas temperature, 150 °C; drying gas flow rate, 15.0 L/min; sheath gas temperature, 350 °C; sheath gas flow rate, 12.0 L/min; capillary voltage, 4500 V (positive)/−4000 V (negative); the mass range was recorded from 50 to 1000 m/z. Agilent Mass Hunter Qualitative Analysis B.08.00 was used for data collection and processing.

Predicting potential targets of QRHX

We identified the 68 chemicals components of QRHX via UPLC-MS analysis. These candidate compounds were imported into the PubChem database (https://pubchem.ncbi.nlm.nih.gov/) to acquire the corresponding canonical simplified molecular input line entry system molecular structures. The chemical formulae of the candidate compounds were also entered into the Swiss Target Prediction (http://www.swisstargetprediction.ch/) Search Server.

Collecting MI-associated targets

We used 'myocardial infarction' as a keyword to identify disease targets related to MI on the DrugBank (https://www.drugbank.ca), Genecard (https://www.genecards.org/), TTD (https://db.idr-blab.org/ttd), OMIM (https://omim.org) and PharmGKB (https://www.pharmgkb.org) databases. The targets in the above databases were integrated, and repeated targets were removed to obtain MI-related targets.

Network construction and merging

We intersected QRHX targets and MI related targets to obtain a common target of both, then imported the targets of QRHX and MI into the BisoGenet module in Cytoscape version 3.8.0 and mapped to protein-protein interaction (PPI) databases, such as the Database of Interacting Proteins, Biological General Repository for Interaction Datasets, Human Protein Reference Database, IntAct Molecular Interaction Database, Molecular INTeraction Database and Biomolecular Interaction Network Database. The PPI network of QRHX and MI-related targets were constructed with Cytoscape software.

Enrichment analysis

We used the Search Tool for the Retrieval of Interacting Genes/Proteins (STRING) database (STRING: functional protein association networks, https://string-db.org/) to analyze the enrichment of the Kyoto Encyclopaedia of Genes and Genomes (KEGG) pathways. Pathways with obvious changes in q value < 0.05 were selected for further evaluation. Genes characterized by remarkably regulated pathways were selected to construct the gene-pathway network for screening key target genes of QRHX in MI.

Rat MI model

All experimental procedures were approved by the Institutional Animal Care Committee of Guangzhou University of Chinese Medicine First Affiliated Hospital (Guangzhou, China). 50 Sprague–Dawley (SD) male rats (180–220 g) were randomly divided into the following four groups ($n = 10$ per group): Sham group, Model group, QRHX low dose group, QRHX medium-dose group and QRHX high dose group. Different doses of QRHX were administered to the latter three groups (5, 10 and 20 g/kg/day, respectively) for 14 days, and saline solution was administered to the model group for 14 days. The rats were anaesthetized via pentobarbital injection (0.4 mL/100 g) and were positioned supine on the operating table. Each animal's chest and neck were shaved and disinfected. Following anaesthesia, the rats underwent intubation and ventilator-assisted ventilation after tracheotomy. The intercostal muscle in the fourth intercostal space (where heartbeats are most readily felt and observed) was separated bluntly using ophthalmic elbow forceps, and a needle holder was used to move the muscles vertically to expose the left anterior decreasing branch. By inserting the needle into the lower edge of the left atrial ear for suture and ligation, the lower end of ligation of the left ventricular can be observed to be pale and the cardiac motion was weakened, indicating the successful ligation. Then close the chest and suture the skin. The endotracheal intubation was removed after spontaneous breathing resumed in the rats. For sham controls, the needle was passed through the myocardium below the LAD artery without a tied suture, and the remainder of the procedure was carried out as written above. 3 days after, the rats were anaesthetized and their hearts were harvested.

Echocardiography

Prior to anaesthesia, cardiac function was assessed using a colour doppler ultrasound. We recorded and calculated the left ventricular ejection fraction (LVEF, %) and left ventricular fractional shortening (LVFS, %).

Histology

Heart tissues were anatomized and fixed using 4% paraformaldehyde, embedded in paraffin, cut into 4 μm sections using a microtome (Leica, Germany), and spread into a 42 °C water bath. Next, deparaffinized, dehydrated and stained with haematoxylin and eosin (H&E), Masson and Sirius red staining. Finally, pathological changes in heart tissues were observed under a light microscope (Leica, Germany).

ELISA

Serum concentrations of the inflammatory factors cTnI, MCP-1, IL-17A, TNF-α, IL-1β were determined with ELISA kits following the manufacturer's recommendations.

Western blot analysis

Cardiac tissues were homogenized by RIPA lysis buffer and the concentration of total proteins was measured by the BCA kit, after which the protein lysates were electrophoresed on 10% SDS-PAGE and transferred onto a polyvinylidene fluoride membrane. Samples were blocked using non-fat milk at 37 °C for 2 h. The membranes were incubated with the primary antibodies at 4 °C overnight and the following secondary antibodies at 37 °C for 1 h in sequence: p-PI3K, PI3K, p-Akt, Akt, LC3B, Beclin-1 and p62. The membranes were washed with TBS-T, Specific protein bands were imaged and quantified by the Image-Pro Plus software. GAPDH levels were used for reference.

Quantitative real-time PCR

Total RNA was extracted from aorta tissues by the miRNeasy Micro Kit. cDNA was inversely transcribed from total RNA by M-MLV Reverse Transcriptase. Quantitative real-time PCR Real-Time System (Bio-Rad, USA) was implemented by the TB Green premix Ex TaqII Mix with targeted primer sets to determine gene expression levels. The sequences of targeted primers are shown in Table 1. Fold-change was calculated by the $2^{-\Delta\Delta Ct}$ method.

Statistical analysis

Data were described as means ± standard error of the mean (SEM) and analyzed by one-way analysis of variance (multiple groups) with SPSS 23.0 (SPSS, USA). The result was displayed by GraphPad Prism 5.0 (GraphPad Prism, USA) software. p-Value < 0.05 represented statistical significance.

Table 1. Sequences of primers used for real-time PCR.

Gene	Forward	Reverse
ATG3	CGGCTCTGGCTGTTTGGCTATG	GGTGGTGGGAGGTGAGGATGG
ATG5	CTCAGCTCTGCCTTGGAACATCAC	AAGTGAGCCTCAACTGCATCCTTG
ATG7	GTGAACCTCAGCGGATGTATGGAC	CCAGCAGCAGGCACTTGACAG
BCL2	GGGCTACGAGTGGGATACTGGAG	TCGGTTGCTCTCAGGCTGGAAG
BAX	GACGCATCCACCAAGAAGCTGAG	GCTGCCCACACGGAAGAAGACC
GAPDH	GGGCTGCCTTCTCTTGTGAC	CCCGTTGATGACCAGCTTCC

Results

Identification of compounds in QRHX

The qualitative analysis results for freeze-dried QRHX powder are shown in Table 2 and quality control of QRHX as shown in Supplementary Figure 1. Target composition standard curve and content test results were listed in Supplementary Tables 1 and 2. We used UPLC-MS analyze a method to profile the chemical constituents of QRHX systematically and comprehensively. The total ion chromatograms of QRHX in both positive and negative ion modes are presented in Figure 2. The retention times and MS data of the characterized compounds are summarised in Table 2. A total of 68 compounds were separated and detected by UPLC-MS (Figure 2(A,B)).

Compound-target network for QRHX

A total of 68 chemical compounds identified in QRHX were selected as candidates. Based on the results of the Swiss Target Prediction Search Server, 223 related targets were obtained (Supplementary Table 3), and the compound-target network was constructed for QRHX (Figure 3). A total of 263 nodes (68 compounds in QRHX and 223 targets) and 398 edges were included in the network, indicating interactions between the compounds and the targets.

Compound-disease-target network

After searching 'myocardial infarction' in DrugBank, Genecard, TTD, OMIM and PharmGKB databases, a total of 2558 disease targets related to MI were obtained (Supplementary Table 4). Then, 223 QRHX targets were intersected with 2558 related targets of MI, and 123 QRHX anti-MI core targets (Supplementary Table 5) were identified by consensus shown in Figure 4(A). Figure 4(B) shows the PPI network of QRHX against MI, which was composed of 122 nodes and 831 edges.

Gene-pathway network

Through enrichment analysis, we obtained 70 pathways significantly associated with QRHX against MI (Supplementary Table 6), including the calcium, PI3K/Akt, cGMP-PKG, HIF-1, sphingolipid, relaxin, estrogen, Rap1, VEGF and PPAR signalling pathways (Figure 5).

QRHX improves cardiac function and inhibits myocardial fibrosis in MI rats

H&E staining demonstrated that rats in the Sham group exhibited no noticeable morphological changes in myocardial tissue. Those in the Model group exhibited morphological changes characterized by disorderly arrangement in myocardial fibres and scattered cytoplasmic staining, whereas myocardial fibrosis was significantly attenuated in the QRHX high dose group compared to the Model group (Figure 6(A)). Collagen deposition was decreased by QRHX compared to the Model group; the high dose is the most significant (Figure 6(B)). Myocardial fibrosis is obvious after myocardial infarction, the situation was significantly ameliorated by QRHX, the high dose is the most significant (Figure 6(C,D)). Cardiac function in the Model group was found to be impaired compared to the Sham group and was manifested by a decrease in LVEF and LVFS. However, the

Table 2. The QRHX freeze-dry powder qualitative analysis results.

No.	RT (min.)	Ion	Observed (m/z)	Formula	Target mass	Diff. (ppm)	Identification
1	0.307	M−	293.2002	$C_{17}H_{27}NO_3$	293.1991	1.67	Nobilonine
2	0.557	(M − H)−	128.035	$C_5H_7NO_3$	129.0426	−2.53	Pyroglutamic acid
3	0.607	(M + HCOO)−	939.1106	$C_{40}H_{30}O_{24}$	894.1127	−0.46	Diellagic acid rhamnoside (1 → 4)glucopyranoside
4	0.607	(M − H)−	939.1106	$C_{41}H_{32}O_{26}$	940.1182	−0.44	1,2,3,4,6-Pentagalloylglucose
5	0.607	(M − H)−	169.0137	$C_7H_6O_5$	170.0215	−3.06	Gallic acid
6	0.623	(M − H)−	615.1004	$C_{28}H_{24}O_{16}$	616.1064	1.99	Desmanthin 2
7	0.623	(M − H)−	717.1446	$C_{36}H_{30}O_{16}$	718.1534	−1.47	Fukugiside
8	0.64	(M − H)−	493.1137	$C_{26}H_{22}O_{10}$	494.1213	−0.74	Salvianolic acid A
9	0.723	(M − H)−	347.1502	$C_{19}H_{24}O_6$	348.1573	0.33	9-Hydroxyglabratolide
10	0.79	(M − H)−	193.0873	$C_{11}H_{14}O_3$	194.0943	1.08	2-Methoxy-4-(3-methoxy-1-propenyl)-phenol
11	0.806	(M − H)−	329.2341	$C_{18}H_{34}O_5$	330.2406	2.45	Sanleng acid
12	0.823	M−	332.2821	$C_{21}H_{36}N_2O$	332.2828	−3.21	Holarrhimine
13	0.823	(M + HCOO)−	329.2341	$C_{17}H_{32}O_3$	284.2351	2.85	Muricatacin
14	0.823	(M − H)−	277.205	$C_{17}H_{28}NO_2$	278.212	1.03	N-Methyldendrobium
15	0.823	(M + HCOO)−	347.1506	$C_{18}H_{22}O_4$	302.1518	2.43	Arnebinone
16	1.022	(M + HCOO)−	243.1597	$C_{12}H_{22}O_2$	198.162	−2.35	cis-4-Dodecenoic acid
17	1.339	M−	315.2569	$C_{21}H_{33}NO$	315.2562	−0.23	Holadysine
18	1.455	M−	297.2096	$C_{20}H_{27}NO$	297.2093	0.18	Spirasine IV
19	2.004	M−	285.2097	$C_{19}H_{27}NO$	285.2093	−0.8	1-Methyl-2-nonyl-4(1H)-quinolone
20	2.985	(M + HCOO)−	643.2548	$C_{36}H_{38}O_8$	598.2567	−0.08	Tinyatoxin
21	3.235	M−	327.2577	$C_{22}H_{33}NO$	327.2562	2.45	1-Methyl-2-dodecyl-4-(1H)-quinolone
22	4.05	(M − H)−	627.2604	$C_{37}H_{40}O_9$	628.2672	0.34	Resiniferotoxin
23	4.832	(M + HCOO)−	561.1779	$C_{30}H_{28}O_8$	516.1784	2.65	Rottlerin
24	5.198	(M + HCOO)−	561.1775	$C_{30}H_{28}O_8$	516.1784	2.	Rottlerin
25	0.604	(M + NH4)+	104.1074	$C_5H_{10}O$	86.0732	4.94	1-Penten-3-ol
26	0.612	M+	118.0989	$C_6H_{14}O_2$	118.0994	0.87	Acetal
27	0.612	(M + NH4)+	360.1496	$C_{12}H_{22}O_{11}$	342.1162	−2.12	Cellobiose
28	0.621	(M + NH4)+	684.2547	$C_{24}H_{42}O_{21}$	666.2219	−1.17	Isolychnose
29	0.687	M+	120.0934	C_9H_{12}	120.0939	0.11	1,2,3-Trimethylbenzene
30	0.945	(M + H)+	124.0397	$C_6H_5NO_2$	123.032	2.5	Nicotinic acid
31	1.145	(M + H)+	139.0392	$C_7H_6O_3$	138.0317	1.73	3,4-Dihydroxybenzyl aldehyde
32	1.427	(M + H)+	197.0809	$C_{10}H_{12}O_4$	196.0736	−0.09	2,4-Dihydroxy-6-methoxy-3-methylacetophenone
33	1.569	(M + H)+	151.039	$C_8H_6O_3$	150.0317	0.04	Piperonal
34	1.868	(M + H)+	182.0959	$C_{13}H_{11}N$	181.0892	−2.55	3-Methylcarbazole
35	1.877	(M + NH4)+	182.0804	$C_9H_8O_3$	164.0473	−4.65	Coumarinic acid
36	1.877	(M + NH4)+	182.0959	$C_{13}H_8$	164.0626	−2.82	1,11-Tridecadiene-3,5,7,9-tetrayne
37	2.093	(M + NH4)+	498.1976	$C_{23}H_{28}O_{11}$	480.1632	−2.27	Albiflorin R1
38	2.093	(M + H)+	197.0802	$C_{10}H_{12}O_4$	196.0736	−3.42	2,4-Dihydroxy-6-methoxy-3-methylacetophenone
39	2.226	(M + NH4)+	104.107	$C_5H_{10}O$	86.0732	0.59	1-Penten-3-ol
40	2.243	(M + H)+	193.0491	$C_{10}H_8O_4$	192.0423	−0.63	6-Methoxy-7-hydroxycoumarin
41	2.326	M+	566.1621	$C_{26}H_{30}O_{14}$	566.1636	−1.75	Angustioside
42	2.342	(M + H)+	123.0804	$C_8H_{10}O$	122.0732	0.06	2,3-Dicresol
43	2.342	(M + H)+	179.0704	$C_{10}H_{10}O_3$	178.063	0.23	Coniferyl aldehyde
44	2.351	(M + H)+	161.0597	$C_{10}H_8O_2$	160.0524	−0.19	1,2-Hydronaphthoquinone
45	2.475	(M + NH4)+	760.3038	$C_{34}H_{46}O_{18}$	742.2684	0.91	(+)-Syringaresinol-di-O-beta-Dglucoside
46	2.642	(M + NH4)+	183.0645	$C_9H_{10}O_4$	182.0579	−3.47	Jacaranone
47	2.658	(M + H)+	169.0858	$C_9H_{12}O_3$	168.0786	−1.31	2-Methoxy-2-(4′-hydroxyphenyl)ethanol
48	2.767	(M + H)+	531.15	$C_{26}H_{26}O_{12}$	530.1424	−0.57	Macranthoin F
49	2.941	(M + H)+	223.0599	$C_{11}H_{10}O_5$	222.0528	−1.75	5,6-Dimethoxy-7-hydroxycoumarin
50	2.966	(M + H)+	417.1176	$C_{21}H_{20}O_9$	416.1107	−0.8	Apigenin-5-rhamnoside
51	2.975	(M + H)+	209.1166	$C_{12}H_{16}O_3$	208.1099	−2.87	1-Allyl-2,4,5-trimethoxy-benzene
52	3.166	(M + H)+	137.0593	$C_8H_8O_2$	136.0524	−2.29	4-Methyl salicylaldehyde
53	3.241	(M + NH4)+	174.1847	$C_{10}H_{20}O$	156.1514	−4.07	1-Methyl-3-isopropoxy cyclohexane
54	3.59	(M + H)+	177.054	$C_{10}H_8O_3$	176.0473	−3.72	6-Hydroxy-7-methylesculetin
55	3.607	(M + H)+	153.055	$C_8H_8O_3$	152.0473	2.22	2,4-Dihydroxyacetophenone
56	3.665	(M + NH4)+	280.1178	$C_{14}H_{14}O_5$	262.0841	−0.5	Celereoin
57	3.806	(M + H)+	153.0547	$C_8H_8O_3$	152.0473	1	2,4-Dihydroxyacetophenone
58	3.84	(M + H)+	289.1066	$C_{16}H_{16}O_5$	288.0998	−1.93	5-Hydroxymethyl-6-endo-3′-methoxy-4′-hydroxyphenyl-8-oxabicyclo[3,2,1]-oct-3-en-2-one
59	3.856	(M + H)+	153.0544	$C_8H_8O_3$	152.0473	−1.9	2,4-Dihydroxyacetophenone
60	3.989	M+	202.215	$C_{10}H_{26}N_4$	202.2158	−1.07	Spermine
61	4.189	(M + H)+	167.0696	$C_9H_{10}O_3$	166.063	−3.86	2,4-Dimethoxybenzaldehyde
62	4.189	(M + H)+	153.0543	$C_8H_8O_3$	152.0473	−1.88	2,4-Dihydroxyacetophenone
63	4.264	(M + H)+	167.0698	$C_9H_{10}O_3$	166.063	−3.1	2,4-Dimethoxybenzaldehyde
64	4.355	(M + H)+	167.0703	$C_9H_{10}O_3$	166.063	0.11	2,4-Dimethoxybenzaldehyde
65	4.447	(M + H)+	163.0384	$C_9H_6O_3$	162.0317	−3.06	3-Hydroxycoumarin
66	4.538	(M + NH4)+	158.1537	$C_9H_{16}O$	140.1201	−1.59	(E)-2-Nonenal
67	4.538	(M + H)+	153.0545	$C_8H_8O_3$	152.0473	−0.41	2,4-Dihydroxyacetophenone
68	4.555	(M + H)+	345.0966	$C_{18}H_{16}O_7$	344.0896	−0.79	3′,4′-Dihydroxywogonin
69	4.597	(M + H)+	137.0601	$C_8H_8O_2$	136.0524	2.21	4-Methyl salicylaldehyde
70	4.73	(M + H)+	171.1371	$C_{10}H_{18}O_2$	170.1307	−4.61	6-alpha-Methyl-2alpha,6betadihydroxymethylbicyclo[3.1.1]heptane
71	4.996	(M + H)+	327.1226	$C_{19}H_{18}O_5$	326.1154	−0.11	2,5-Dimethoxy-4-hydroxy-[2″,3″:7,8]-furanoflavan
72	5.037	(M + H)+	175.1113	$C_{12}H_{14}O$	174.1045	−3.06	4,7-Dimethyl-1-tetralone
73	5.046	(M + H)+	137.0595	$C_8H_8O_2$	136.0524	−1.12	4-Methyl salicylaldehyde

(continued)

Table 2. Continued.

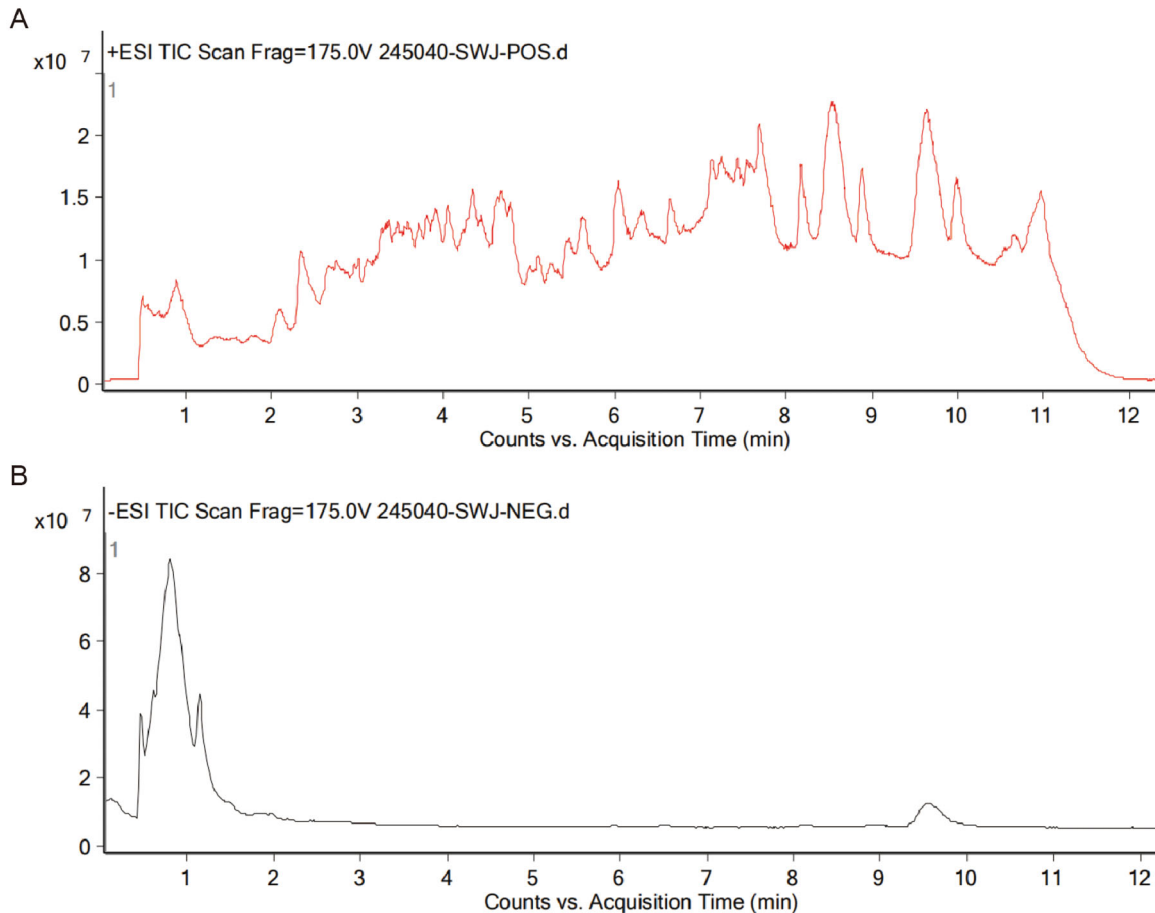| No.	RT (min.)	Ion	Observed (m/z)	Formula	Target mass	Diff. (ppm)	Identification
74	6.019	(M + NH4)+	282.1227	$C_{16}H_{12}N_2O_2$	264.0899	−3.56	Nauclefidine
75	6.718	(M + H)+	409.3835	$C_{30}H_{48}$	408.3756	1.61	Neohopadiene
76	11.193	(M + H)+	195.1375	$C_{12}H_{18}O_2$	194.1307	−1.7	(+)-Myrtenyl acetate
77	12.1	(M + H)+	118.0861	$C_5H_{11}NO_2$	117.079	−1.16	Betaine
78	12.1	(M + NH4)+	118.0861	$C_5H_8O_2$	100.0524	−1.35	Tiglic acid

Figure 2. Total ion chromatograms of QRHX analysed by UPLC-MS. (A) Positive ion mode; (B) Negative ion mode.

cardiac function was improved in the different doses of QRHX groups compared to the Model group, among them QRHX high dose group had a remarkable curative effect (Figure 6(E)). Compared with the sham group, the myocardial infarction marker cTnI in the model group was significantly higher, and the level of cTnI in each QRHX-H group was lower than that in the model group (Figure 6(F)).

QRHX mediates P13K/Akt signal pathway to regulate the level of inflammatory cytokines

MCP-1, IL-17A, TNF-α and IL-1β levels (Figure 7(A)) in the Model group were increased remarkably compared to the Sham group. Compared with the Model group, the MCP-1 level in the QRHX-L group was down-regulated, and the downward trend was more significant in the QRHX-M and QRHX-H groups. IL-

17A inflammatory factor level in each QRHX group showed a huge decrease over the Model group. TNF-α was noticeably lower in QRHX-M and QRHX-H groups than Model group. The IL-1β level is also remarkably reduced in the QRHX-H group. Meanwhile, western blot results demonstrated that p-PI3K/PI3K and p-Akt/Akt levels increased in the Model group compared to the Sham group. QRHX treatment down-regulated the expression levels of p-PI3K/PI3K and p-Akt/Akt (Figure 7(B,C)), QRHX high dose group had the most curative effect.

QRHX plays a protective role in myocardium by regulating autophagy

Western blot results demonstrated that LC3B and Beclin-1 levels decreased while p62 levels increased in the Model group compared to the Sham group. QRHX treatment upregulated the
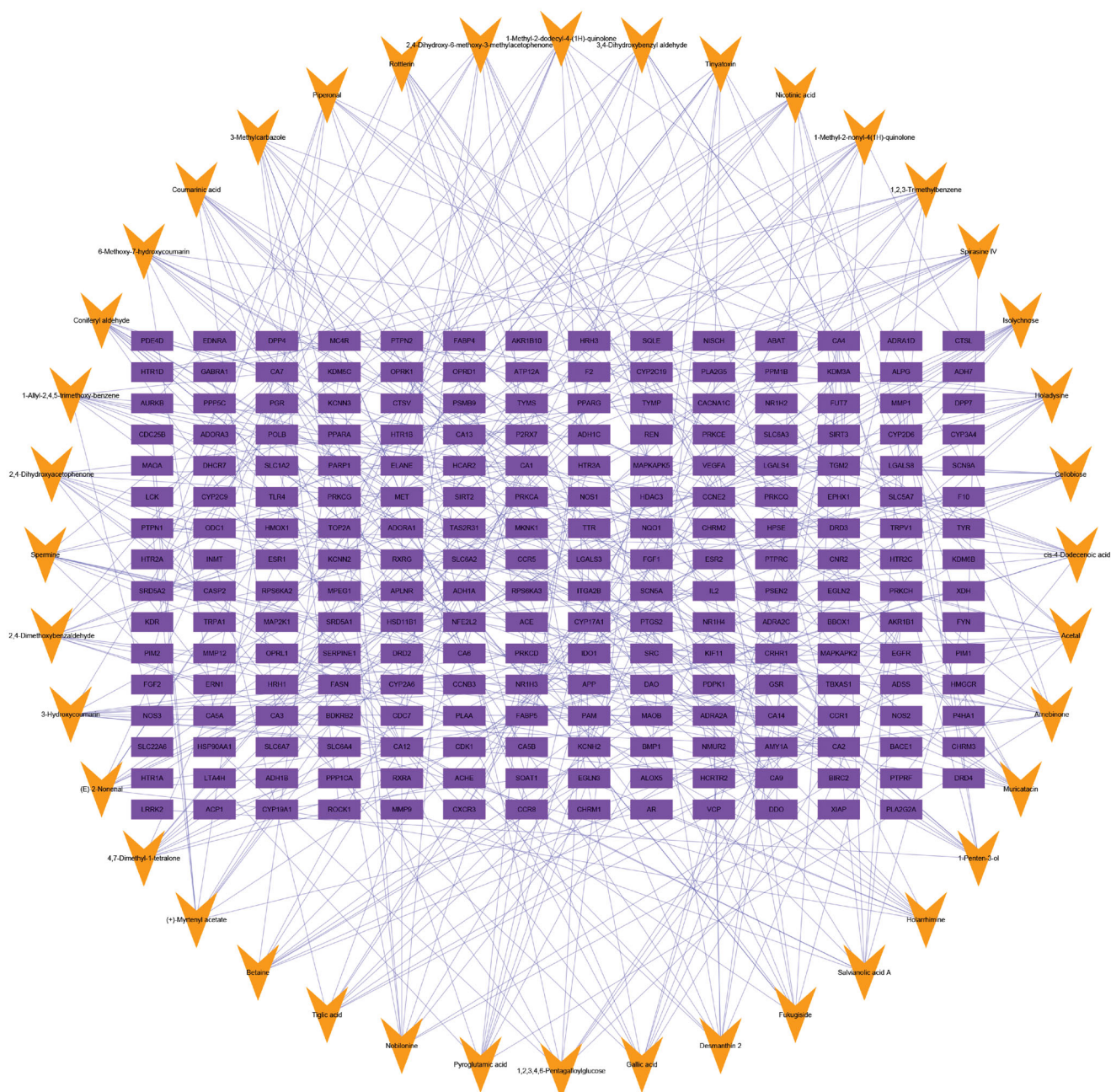
Figure 3. Compound-target network for QRHX. The purple rectangles represent targets; the orange triangle represent QRHX compounds.

expression levels of LC3B and Beclin-1 and prevented an increase in p62 levels (Figure 8(A,B)), and the QRHX high dose group had the most curative effect. Autophagy-related molecules, compared to the Sham group, mRNA expression levels of ATG3, ATG5, ATG7, BCL2/BAX were reduced in the Model group. Compared with the model group, ATG3, BCL2/BAX levels were up-regulated in the QRHX-H group. Moreover, ATG5 and ATG7 levels were significantly increased in both QRHX-M and QRHX-H groups compared with the model group (Figure 8(C)).

Discussion

MI is a serious cardiovascular disease. Despite the sustained optimization of modern medical devices and drug therapy, MI is still associated with complications that significantly impact the quality of life and lead to death. After 1000 years of inheritance and development, TCM, based on its unique theory, can be applied for diseases intervention via a combination of various compounds, focussing on functional recovery and etiology elimination with positive curative effects. Therefore, integrated treatments based in TCM and western medicine have promising prospects. QRHX is composed of seven TCM compounds, but its specific mechanism of action in treating MI has not been systematically elucidated. This study aimed to explore the components and mechanism of QRHX using network pharmacology methods.

Impaired suppression of postinfarction inflammation, perturbed spatial containment of the inflammatory response, and overactive fibrosis may cause adverse remodelling in patients with infarction, contributing to the pathogenesis of heart failure

A

B
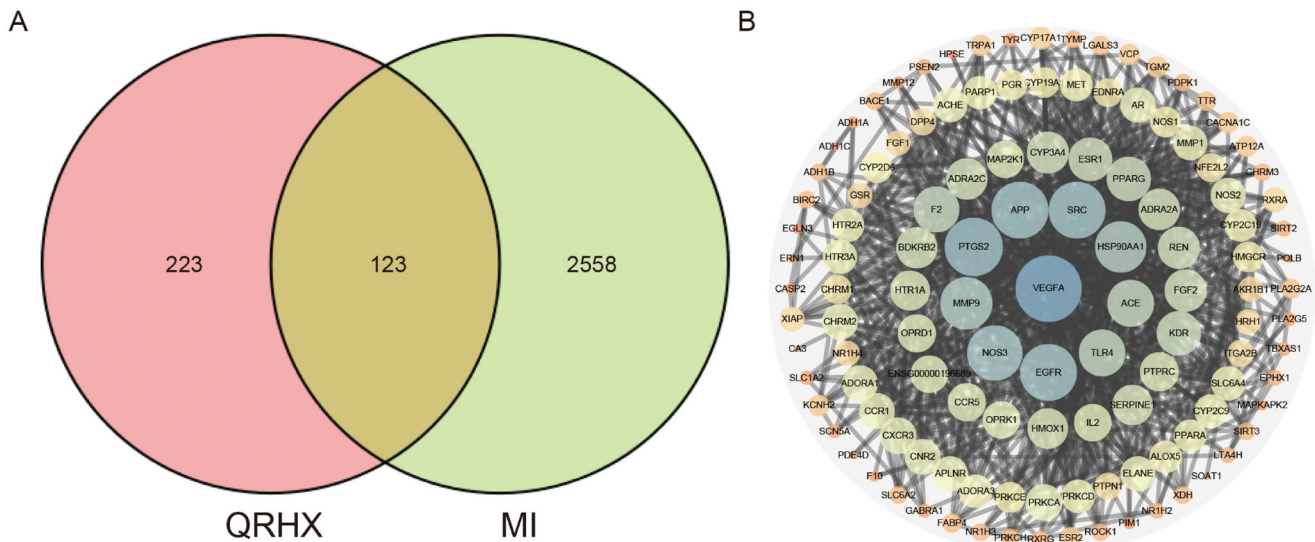
Figure 4. Network pharmacology of QRHX against MI. (A) Venn diagram of QRHX and MI- related targets. (B) PPI network of QRHX in MI treatment.
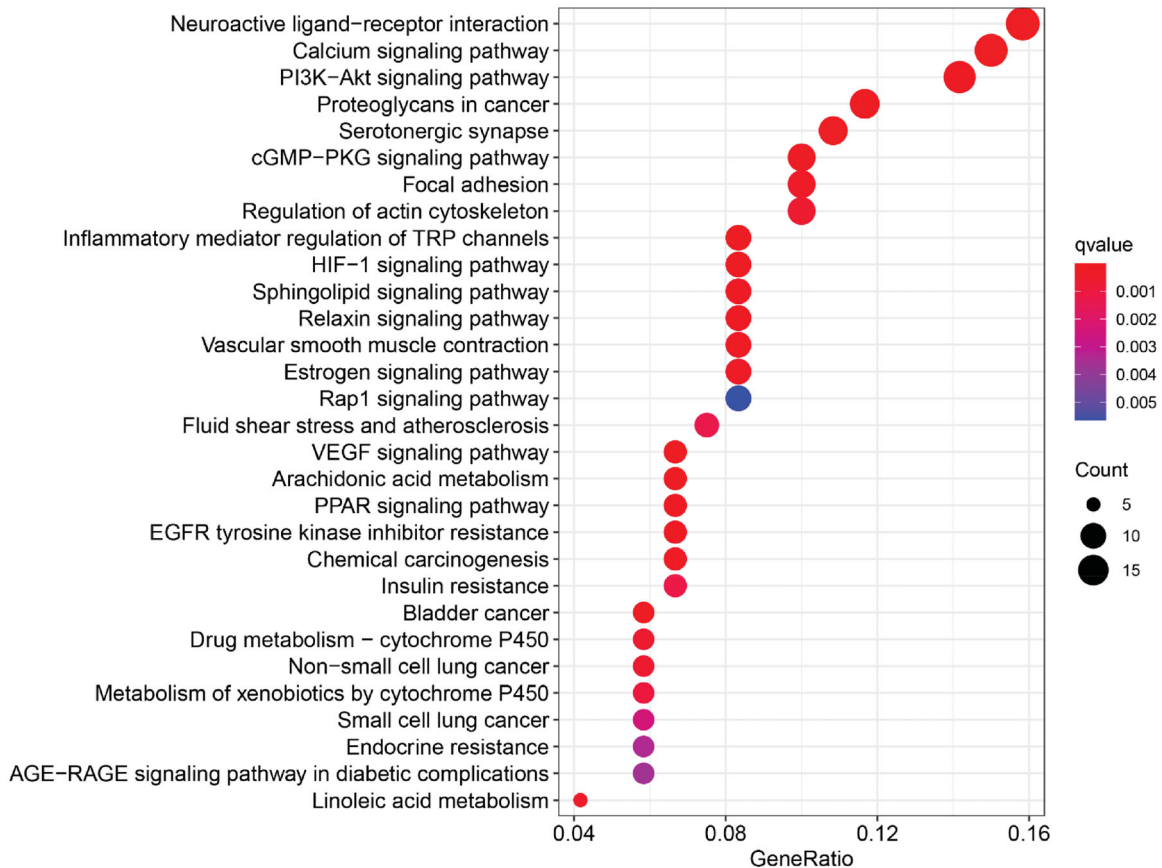

Figure 5. Target-pathway network for QRHX in MI treatment.

(Francis Stuart et al. 2016; Prabhu and Frangogiannis 2016; Talman and Ruskoaho 2016). Lost cells that died in response to ischaemia in MI are replaced by a fibrotic scar, followed by remodelling of the surrounding myocardium and eventually leads to decreased cardiac function (Sutton and Sharpe 2000; Laflamme and Murry 2005). Our results showed that the anti-MI effects of QRHX were related to down-regulate the fibrotic levels in MI rats. We found that cardiac function in the Model group was impaired and characterized by a decrease in LVEF and LVFS determined by cardiac colour ultrasound. Compared to the Model group, the cardiac function of rats in the QRHX groups was improved, especially in the high-dose QRHX group. By using H&E, Masson and Sirius red staining, we found that the Model group manifested a disordered arrangement of myocardial fibres, scattered cytoplasmic staining, obvious deposition of myocardial interstitial collagen, and abundant fibroblasts. However, the proliferation of myocardial fibroblasts and the degree of myocardial interstitial fibrosis were significantly reduced in the QRHX treatment groups, indicating inhibiting treatment of QRHX in post-MI cardiac fibrosis.
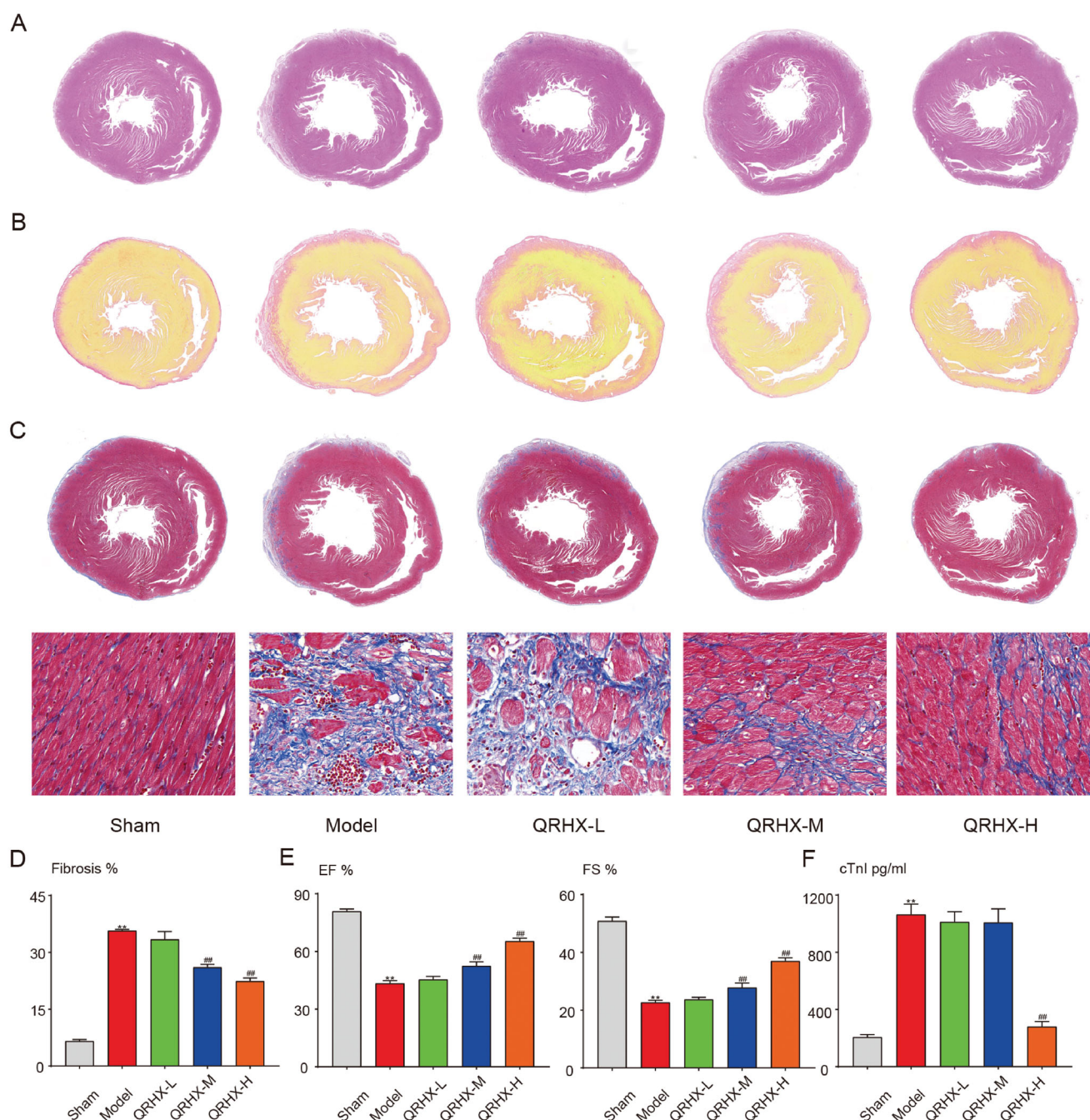
Figure 6. QRHX improves cardiac function and reduces the fibrosis area in MI rats. (A) H&E staining, (B) Sirius red staining, (C) Masson staining of heart tissue. (D) Area of fibrosis in each group. (E) LVEF and LVFS levels of rats in each group. (F) Myocardial infarction marker level of cTnI. Data were expressed as mean ± SEM. **$p < 0.01$ vs. Normal group, #$p < 0.05$ and ##$p < 0.01$ vs. Model group.

This study used a network pharmacology approach combined with UPLC-MS to identify the mechanisms by which QRHX may ameliorate MI. In total, 68 components were obtained from freeze-dried QRHX powder by UPLC-MS, and 223 targets were obtained by PubChem and Swiss. Additionally, 2558 MI-related targets were obtained from DrugBank, Genecard, TTD, OMIM and PharmGKB databases. Finally, we obtained 123 targets from the intersection of the above two targets, and bioinformatics analysis was performed to explore the mechanism underlying anti-MI effects of QRHX. QRHX is a multi-component and multi-target formulation used to treat MI. A total of 70 KEGG signalling pathways were obtained, including the PI3K/Akt signalling pathway, which was significantly enriched.

MI is an inflammatory vascular disease, and inflammatory cell infiltration plays a major role in the pathological manifestation of MI (Crea and Libby 2017; Ong et al. 2018). During the inflammatory phase, increased myocardial levels of TNF and MCP-1 are associated with mortality and dilative remodelling in animals undergoing reperfused infarction protocols (Zymek et al. 2007). In the late remodelling stages, IL-17A functions by promoting sustained infiltration of neutrophils and macrophages (Yan et al. 2012). Impaired suppression of postinfarction inflammation and overactive fibrosis may cause adverse remodelling in patients with infarction, which contributes to heart failure. Massive sudden loss of cardiomyocytes after infarction overwhelms the limited regenerative capacity of the myocardium,
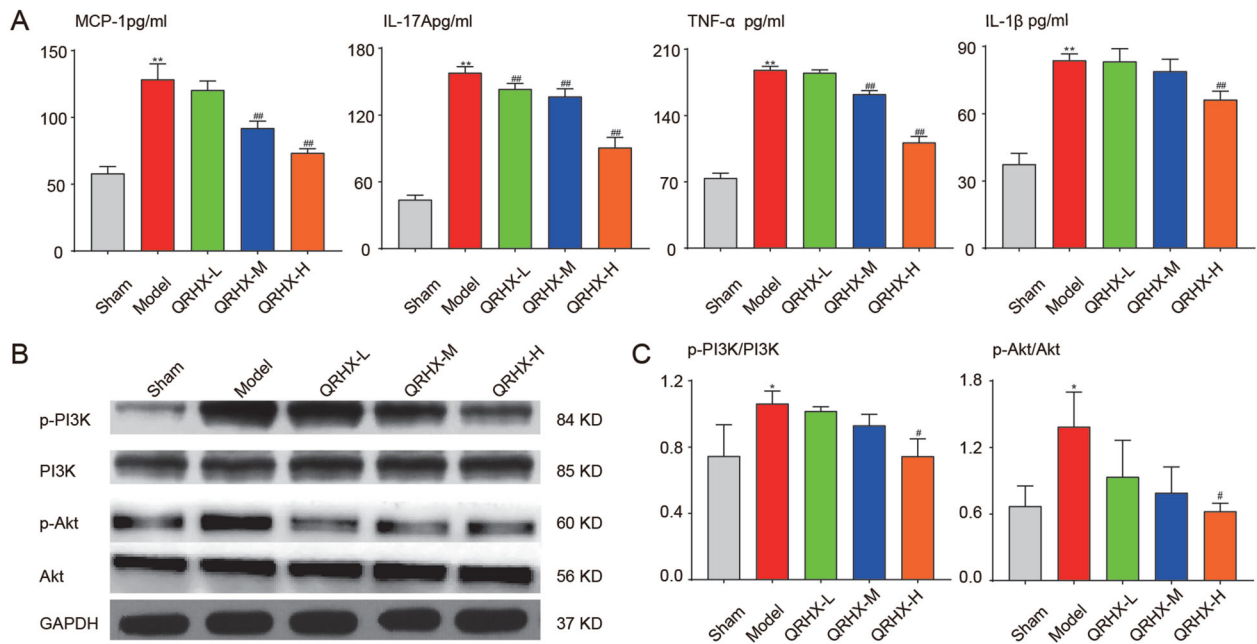
Figure 7. QRHX inhibits PI3K/Akt signal pathway and down-regulates the level of inflammatory cytokines. (A) Inflammatory factor levels of MCP-1, IL-17A, TNF-α and IL-1β. (B) Protein expression levels of p-PI3K, PI3K, p-Akt and Akt. (C) Quantitative analysis of p-PI3K, PI3K, p-Akt and Akt using ImageJ software. Data were expressed as mean ± SEM. **$p < 0.01$ vs. Normal group, #$p < 0.05$ and ##$p < 0.01$ vs. Model group.
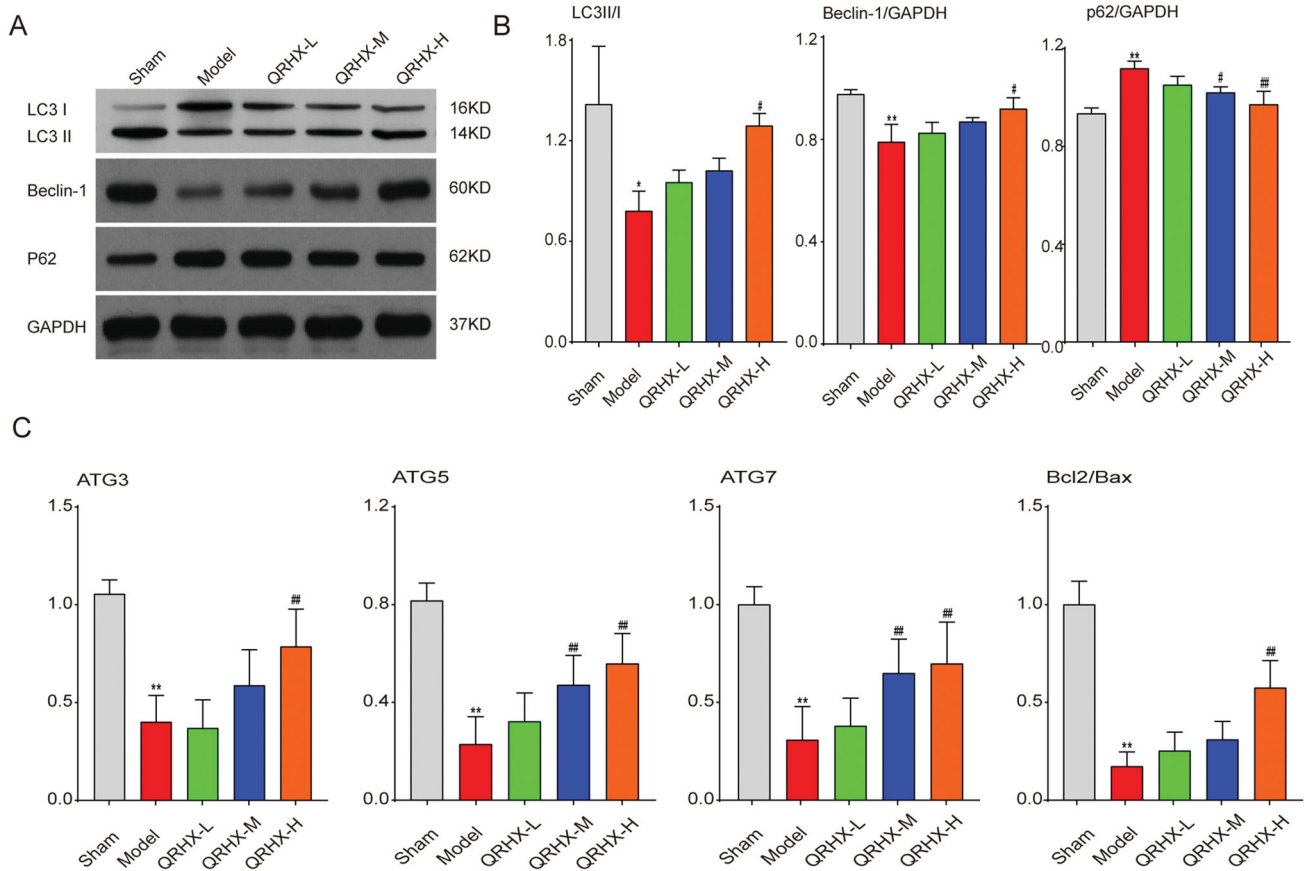
Figure 8. QRHX activated autophagy to exert myocardial protective function. (A) Protein expression levels of LC3B, Beclin-1, p62. (B) Quantitative analysis of LC3B, Beclin-1, p62 using ImageJ software. (C) mRNA expression levels of ATG3, ATG5, ATG7, Bcl2/Bax. Data were expressed as mean ± SEM. **$p < 0.01$ vs. Normal group, #$p < 0.05$ and ##$p < 0.01$ vs. Model group.

leading to the formation of a collagen-based scar. It is widely accepted that the PI3K/Akt pathway is crucial in cell survival and inflammation regulation and drives the secretion of a large panel of pro-inflammatory cytokines. IL-17A plays a pathogenic role both in the early and late stages of post-MI remodelling, and promotes cell proliferation and migration via PI3K/Akt1/NF-κB-p65 activation (Wang et al. 2019). In our study, compared to the Model group, represented by QRHX high dose group, QRHX groups showed varying degrees of decline in the expression of inflammatory cytokines IL-17A, TNF-α, IL-1β and chemokines MCP-1, implicating the inhibitory effect of QRHX against inflammation.

Autophagic activity has been shown to decrease during MI, which exacerbates inflammation and aggravates cardiac remodelling after MI (Sciarretta et al. 2018). Our conclusion suggested that QRHX could up-regulate the expression of autophagy-related proteins LC3B and Beclin-1, and down-regulate the expression of p62. In addition, QRHX can improve the expression of autophagy-related genes ATG3, ATG5, ATG7, BCL2/BAX to different degrees at the molecular level. Moreover, QRHX has been found to activate the autophagy of macrophages. The phenomenon in which autophagy occurs after various subsets of inflammatory cells accumulate, exhibiting varying functional capability in MI is attracted extensive attention. Previous studies have shown that the PI3K/Akt signalling pathway affects the occurrence and development of MI by participating in myocardial cell apoptosis and autophagy (Li et al. 2019; Zhang, Liang, et al. 2019; Zhao et al. 2019). Therefore, we speculated that QRHX may activate autophagy to exert myocardial protective function. Our findings indicate that QRHX caused a significant decrease in p-PI3K and p-Akt with increasing doses as shown by western blot analysis, indicating that the inhibition of the PI3K/Akt pathway is correlated with activated autophagy activation and decreased inflammation. Therefore, we speculated that QRHX may exert a protective myocardial effect by activating autophagy and suppressing inflammation via the PI3K/Akt pathway.

Conclusion

In this study, we employed a network pharmacology approach combined with UPLC-MS to identify the mechanisms by which QRHX ameliorates MI. We found that QRHX plays a role in myocardial protection by activating autophagy and partially downregulating cardiomyocyte inflammation via the PI3K/Akt signalling pathway. QRHX could potentially target multiple targets either directly or indirectly to have a synergistic effect on anti-MI. However, additional studies are required to further delineate the mechanistic actions of QRHX on MI.

Acknowledgements

Disclosure statement

No potential conflict of interest was reported by the author(s).

Funding

ORCID

Junfeng Fang ⓘ http://orcid.org/0000-0003-4235-4520
Wei Wu ⓘ http://orcid.org/0000-0001-8911-6920

References

Bai YD, Yang YR, Mu XP, Lin G, Wang YP, Jin S, Chen Y, Wang MJ, Zhu YC. 2018. Hydrogen sulfide alleviates acute myocardial ischemia injury by modulating autophagy and inflammation response under oxidative stress. Oxid Med Cell Longev. 2018:3402809.

Cai W, Shen WD. 2018. Anti-apoptotic mechanisms of acupuncture in neurological diseases: a review. Am J Chin Med. 46(3):515–535.

Crea F, Libby P. 2017. Acute coronary syndromes: the way forward from mechanisms to precision treatment. Circulation. 136(12):1155–1166.

Emanuele E, Minoretti P, Sanchis-Gomar F, Pareja-Galeano H, Yilmaz Y, Garatachea N, Lucia A. 2014. Can enhanced autophagy be associated with human longevity? Serum levels of the autophagy biomarker beclin-1 are increased in healthy centenarians. Rejuvenation Res. 17(6):518–524.

Escobar M, Echeverría O, Vázquez-Nin G. 2013. Role of autophagy in the ovary cell death in mammals. In: Bailly Y, editor. Autophagy-a double-edged sword-cell survival or death. London (UK): Intech Open; p. 423–441.

Fan S, Zhang J, Xiao Q, Liu P, Zhang Y, Yao E, Chen X. 2020. Cardioprotective effect of the polysaccharide from *Ophiopogon japonicus* on isoproterenol-induced myocardial ischemia in rats. Int J Biol Macromol. 147:233–240.

Francis Stuart SD, De Jesus NM, Lindsey ML, Ripplinger CM. 2016. The crossroads of inflammation, fibrosis, and arrhythmia following myocardial infarction. J Mol Cell Cardiol. 91:114–122.

Hao P, Jiang F, Cheng J, Ma L, Zhang Y, Zhao Y. 2017. Traditional Chinese medicine for cardiovascular disease: evidence and potential mechanisms. J Am Coll Cardiol. 69(24):2952–2966.

Ibanez B, James S, Agewall S, Antunes MJ, Bucciarelli-Ducci C, Bueno H, Caforio ALP, Crea F, Goudevenos JA, Halvorsen S, et al. 2018. 2017 ESC Guidelines for the management of acute myocardial infarction in patients presenting with ST-segment elevation: the task force for the management of acute myocardial infarction in patients presenting with ST-segment elevation of the European Society of Cardiology (ESC). Eur Heart J. 39(2):119–177.

Jia D, Zhang CZ, Qiu Y, Chen XF, Jia L, Chen AF, Chai YF, Zhu ZY, Huang J, Zhang C. 2019. Cardioprotective mechanisms of salvianic acid a sodium in rats with myocardial infarction based on proteome and transcriptome analysis. Acta Pharmacol Sin. 40(12):1513–1522.

Jiang T, Harder B, Rojo de la Vega M, Wong PK, Chapman E, Zhang DD. 2015. p62 links autophagy and Nrf2 signaling. Free Radic Biol Med. 88(B):199–204.

Laflamme MA, Murry CE. 2005. Regenerating the heart. Nat Biotechnol. 23(7):845–856.

Li T, Tian H, Li J, Zuo A, Chen J, Xu D, Guo Y, Gao H. 2019. Overexpression of lncRNA Gm2691 attenuates apoptosis and inflammatory response after myocardial infarction through PI3K/Akt signaling pathway. IUBMB Life. 71(10):1561–1570.

Li X, Yuan T, Chen D, Chen Y, Sun S, Wang D, Fang L, Lu Y, Du G. 2018. Cardioprotective effects of puerarin-V on isoproterenol-induced myocardial infarction mice is associated with regulation of PPAR-Y/NF-κB pathway. Molecules. 23(12):3322.

Li YY, Zhao YH. 2017. Efficacy and mechanisms of Chinese medicine on the modulation of myocardial autophagy in cardiovascular disease. Am J Chin Med. 45(5):917–932.

Ma S, Wang Y, Chen Y, Cao F. 2015. The role of the autophagy in myocardial ischemia/reperfusion injury. Biochim Biophys Acta. 1852(2):271–276.

Mohajeri M, Sahebkar A. 2018. Protective effects of curcumin against doxorubicin-induced toxicity and resistance: a review. Crit Rev Oncol Hematol. 122:30–51.

Mourouzis K, Oikonomou E, Siasos G, Tsalamadris S, Vogiatzi G, Antonopoulos A, Fountoulakis P, Goliopoulou A, Papaioannou S,

Tousoulis D. 2020. Pro-inflammatory cytokines in acute coronary syndromes. Curr Pharm Des. 26(36):4624–4647.

Ong SB, Hernández-Reséndiz S, Crespo-Avilan GE, Mukhametshina RT, Kwek XY, Cabrera-Fuentes HA, Hausenloy DJ. 2018. Inflammation following acute myocardial infarction: multiple players, dynamic roles, and novel therapeutic opportunities. Pharmacol Ther. 186:73–87.

Prabhu SD, Frangogiannis NG. 2016. The biological basis for cardiac repair after myocardial infarction: from inflammation to fibrosis. Circ Res. 119(1):91–112.

Ren G, Dewald O, Frangogiannis NG. 2003. Inflammatory mechanisms in myocardial infarction. Curr Drug Targets Inflamm Allergy. 2(3):242–256.

Roffi M, Patrono C, Collet JP, Mueller C, Valgimigli M, Andreotti F, Bax JJ, Borger MA, Brotons C, Chew DP, et al. 2016. 2015 ESC Guidelines for the management of acute coronary syndromes in patients presenting without persistent ST-segment elevation: task force for the management of acute coronary syndromes in patients presenting without persistent ST-segment elevation of the European society of cardiology (ESC). G Ital Cardiol. 17:831–872.

Ryter SW, Bhatia D, Choi ME. 2019. Autophagy: a lysosome-dependent process with implications in cellular redox homeostasis and human disease. Antioxid Redox Signal. 30(1):138–159.

Sciarretta S, Yee D, Nagarajan N, Bianchi F, Saito T, Valenti V, Tong M, Del Re DP, Vecchione C, Schirone L, et al. 2018. Trehalose-induced activation of autophagy improves cardiac remodeling after myocardial infarction. J Am Coll Cardiol. 71(18):1999–2010.

Shinde AV, Frangogiannis NG. 2014. Fibroblasts in myocardial infarction: a role in inflammation and repair. J Mol Cell Cardiol. 70:74–82.

Sutton MGSJ, Sharpe N. 2000. Left ventricular remodeling after myocardial infarction: pathophysiology and therapy. Circulation. 101(25):2981–2988.

Talman V, Ruskoaho H. 2016. Cardiac fibrosis in myocardial infarction-from repair and remodeling to regeneration. Cell Tissue Res. 365(3):563–581.

Thygesen K, Alpert JS, Jaffe AS, Chaitman BR, Bax JJ, Morrow DA, White HD, Thygesen K, Alpert JS, Jaffe AS, et al. 2019. Fourth universal definition of myocardial infarction (2018). Eur Heart J. 40(3):237–269.

Tousoulis D, Antoniades C, Koumallos N, Stefanadis C. 2006. Pro-inflammatory cytokines in acute coronary syndromes: from bench to bedside. Cytokine Growth Factor Rev. 17(4):225–233.

Wang L, Li Y, Ning N, Wang J, Yan Z, Zhang S, Jiao X, Wang X, Liu H. 2018. Decreased autophagy induced by β (1)-adrenoceptor autoantibodies contributes to cardiomyocyte apoptosis. Cell Death Dis. 9(3):1–13.

Wang B, Zhao C-H, Sun G, Zhang Z-W, Qian B-M, Zhu Y-F, Cai M-Y, Pandey S, Zhao D, Wang Y-W, et al. 2019. IL-17 induces the proliferation and migration of glioma cells through the activation of PI3K/Akt1/NF-κB-p65. Cancer Lett. 447:93–104.

Xiu WJ, Yang HT, Zheng YY, Ma YT, Xie X. 2018. Drug-eluting balloons versus second-generation drug-eluting stents for treating in-stent restenosis in coronary heart disease after PCI: a meta-analysis. Cardiol Res Pract. 2018:7658145.

Yan X, Shichita T, Katsumata Y, Matsuhashi T, Ito H, Ito K, Anzai A, Endo J, Tamura Y, Kimura K. 2012. Deleterious effect of the IL-23/IL-17 a axis and γδ T cells on left ventricular remodeling after myocardial infarction. J Am Heart Assoc. 1:e004408.

Zhang C, Liang R, Gan X, Yang X, Chen L, Jian J. 2019. MicroRNA-384-5p/Beclin-1 as potential indicators for epigallocatechin gallate against cardiomyocytes ischemia reperfusion injury by inhibiting autophagy via PI3K/Akt pathway. Drug Des Devel Ther. 13:3607–3623.

Zhang L, Liu P, Wen W, Bai X, Zhang Y, Liu M, Wang L, Wu Y, Yuan Z, Zhou J. 2019. IL-17A contributes to myocardial ischemic injury by activating NLRP3 inflammasome in macrophages through AMPKα/p38MAPK/ERK1/2 signal pathway in mice. Mol Immunol. 105:240–250.

Zhao L, Yang XR, Han X. 2019. MicroRNA-146b induces the PI3K/Akt/NF-κB signaling pathway to reduce vascular inflammation and apoptosis in myocardial infarction by targeting PTEN. Exp Ther Med. 17(2):1171–1181.

Zuo Q, Chu QM, Jin Z, Li JL, Wu W. 2021. [Qingre Huoxue recipe for treatment of acute ST segment elevation myocardial infarction: a prospective multicenter cohort study]. J Trad Chinese Med. 62(03):229–234. Chinese.

Zymek P, Nah D-Y, Bujak M, Ren G, Koerting A, Leucker T, Huebener P, Taffet G, Entman M, Frangogiannis NG. 2007. Interleukin-10 is not a critical regulator of infarct healing and left ventricular remodeling. Cardiovasc Res. 74(2):313–322.